Electronic Supplementary Material (ESI) for Energy & Environmental Science.

Supplementary Information for:

570 mV Photovoltage, Stabilized n-Si/CoO$_x$ Heterojunction Photoanodes Fabricated Using Atomic Layer Deposition

Xinghao Zhou[1,2], Rui Liu[1], Ke Sun[1,3], Kimberly M. Papadantonakis[1,3], Bruce S. Brunschwig[1,4], Nathan S. Lewis[1,3,4,5*]

[1]Joint Center for Artificial Photosynthesis, California Institute of Technology, Pasadena, CA 91125, USA

[2]Division of Engineering and Applied Science, Department of Applied Physics and Materials Science, California Institute of Technology, Pasadena, CA 91125, USA

[3]Division of Chemistry and Chemical Engineering, California Institute of Technology, Pasadena, CA 91125, USA

[4]Beckman Institute and Molecular Materials Research Center, California Institute of Technology, Pasadena, CA 91125, USA

[5]Kavli Nanoscience Institute, California Institute of Technology, Pasadena, CA 91125, USA

*Corresponding author: nslewis@caltech.edu

Experimental Details:

Materials and Chemicals:

Sulfuric acid (H_2SO_4, Mallinckrodt Chemicals, ACS Reagent grade, 95%-98%), concentrated hydrochloric acid (HCl, EMD, ACS Reagent grade, 36.5-38%), hydrogen peroxide (H_2O_2, Macron Chemicals, ACS grade 30%), potassium hydroxide pellets (KOH, Macron Chemicals, ACS 88%), buffered HF improved (Transene Company Inc.), potassium chloride (KCl, Macron Chemicals, Granular ACS 99.6%), potassium ferrocyanide trihydrate ($K_4Fe(CN)_6 \bullet 3H_2O$, Acros, >99%), and potassium ferricyanide ($K_3Fe(CN)_6$, Fisher Chemicals, certified ACS 99.4%) were used as received except where noted otherwise. Water with a resistivity $\geqslant$ 18 MΩ·cm was obtained from a Barnsted Nanopure deionized (DI) water system.

Acetonitrile (CH_3CN, anhydrous, Sigma-Aldrich, 99.8%) was dried by flowing the solvent through a column of activated Al_2O_3, followed by storage over 3 Å activated molecular sieves (Sigma-Aldrich), for non-aqueous electrochemistry. Lithium perchlorate ($LiClO_4$, Sigma-Aldrich, battery grade 99.99%) was dried at 300 K under a pressure $< 1 \times 10^{-3}$ Torr. Bis(cyclopentadienyl) iron(II) (ferrocene, $FeCp_2$, Sigma-Aldrich), bis(pentamethylcyclopentadienyl)iron ($Me_{10}Cp_2Fe$, decamethyl ferrocene, Strem, 99%) and bis(cyclopentadienyl)cobalt(II) (Cp_2Co, cobaltocene, Strem, 98%) were purified by sublimation under vacuum. Bis(cyclopentadienyl) iron(III) tetrafluoroborate (ferrocenium, $FeCp_2^+ BF_4^-$, Sigma Aldrich, technical grade), and bis(cyclopentadienyl)cobalt(III) hexafluorophosphate (cobaltocenium hexafluorophosphate, $CoCp_2^+PF_6^-$, Sigma-Aldrich, 98%) were recrystallized from diethyl ether (EMD, ACS grade) and CH_3CN (EMD Chemicals, ACS grade), and dried under vacuum. Bis(pentamethylcyclopentadienyl)ferrocenium tetrafluoroborate (decamethylferrocenium, $Me_{10}Fe^+BF_4^-$) and bis(methylcyclopentadienyl)iron tetrafluoroborate ($Me_2Cp_2Fe^+BF_4^-$) were synthesized by chemical oxidation of the neutral metallocenes.[1]

Preparation of substrates:

Degenerately boron-doped (p^+-type, (100)-oriented, single-side polished, resistivity < 0.005 ohm cm) and phosphorus-doped (n-type, (100)-oriented, single-side polished, resistivity 0.1-1 ohm cm) Si wafers were purchased from Addison Engineering Inc. The Si surfaces were first cleaned using a piranha etching procedure that involved soaking the Si wafers in a 3:1 (by volume) solution of H_2SO_4 and H_2O_2 for 10 min, and then placing the Si wafers in a buffered HF etchant for 1 min. The Si wafers were then etched using an RCA SC-2 procedure consisting of soaking the Si wafers in a solution of H_2O, concentrated hydrochloric acid and hydrogen peroxide (5:1:1 by volume) at 75 °C for 10 min. The Si wafers were then thoroughly rinsed using deionized water and dried under a flow of $N_2(g)$. The process produced a thin layer of SiO_x ($SiO_{x,RCA}$) on the surface of Si wafers. n-CdTe(111) (carrier concentration 5.5×10^{17} cm^{-3}) wafers were first etched for 30 s in a freshly prepared 0.5% solution of Br_2 (Sigma Aldrich, 99.999%) in CH_3OH (EMD Millipore, > 99.9%), then rinsed vigorously with CH_3OH, and dried with $N_2(g)$.

Atomic-layer deposition of cobalt oxides:

CoO_x films were deposited onto Si substrates at 150 °C using an Ultratech Fiji ALD system. The cobaltocene precursor was heated and maintained at 80 °C. Each ALD cycle consisted of a 2 s pulse of the cobaltocene precursor, a 10 s purge under a 20 cm^3 min^{-1} flow of research-grade $N_2(g)$, a 5 s ozone pulse and another 10 s $N_2(g)$ purge. 1000 ALD cycles were used for cobalt oxide coatings on Si and CdTe wafers.

Preparation of electrodes:

Ohmic contacts to the back sides of the Si samples were formed by scribing an In-Ga alloy (Alfa Aesar, 99.99%) onto the unpolished surfaces. The In-Ga contact was then attached to a coiled, tin-plated Cu wire (McMaster-Carr) using high purity Ag paste (SPI supplies). The Cu wire was threaded through a glass tube (Corning Inc., Pyrex tubing, 7740 glass), and the samples were encapsulated and sealed to the glass tube using grey epoxy (Hysol 9460F). A high-resolution optical scanner (Epson Perfection V370 with a resolution of 2400 psi) was used to image the exposed surface area of each electrode, and the areas were measured using ImageJ software. All of the electrodes were ~0.1 cm^2 in area, unless specified otherwise.

Electrochemical Measurements:

For electrochemical measurements performed using 1.0 M KOH(aq) as an electrolyte, including photoelectrochemical, spectral response, and Faradaic efficiency measurements, a mercury/mercury oxide (Hg/HgO in 1.0 M KOH(aq), CH Instruments, CHI152) electrode was used as the reference electrode, and a carbon rod placed within a fritted glass tube (gas dispersion tube Pro-D, Aceglass, Inc.) was used as the counter electrode. The Hg/HgO reference electrode was calibrated versus the reversible hydrogen electrode, RHE, and the Hg/HgO electrode potential was determined to be 0.925 V vs. RHE. For electrochemical measurements performed in 50 mM $K_3Fe(CN)_6$, 350 mM $K_4Fe(CN)_6$ and 1.0 M KCl as well as electrochemical measurements in non-aqueous solutions, a Pt wire (0.5 mm diameter, 99.99% trace metal basis, Alfa, Aesar) was used as the reference electrode and a Pt gauze was used as the counter electrode. A custom electrochemical cell with a flat glass (Pyrex) bottom was used for all of the electrochemical measurements. During measurements, the electrolyte was rigorously agitated with a magnetic stir bar driven by a model-train motor (Pittman). The data presented for electrochemical measurements of n-Si did not include compensation for the series resistance of the solution, while the current-density versus potential curve for n-CdTe/CoO_x photoanode included 80% compensation for the series resistance of the solution. A solar simulator with a Xe lamp (Newport 67005 and 69911), as well as ELH-type (Sylvania/Osram) and ENH-type (EIKO) tungsten-halogen lamps were used for photoelectrochemical experiments. The illumination intensity at the position of the working electrode was determined by placing a Si photodiode (FDS100-Cal, Thorlabs) in the cell, in the same position as the exposed area of the photoelectrode. A broadband reflection mirror (Newport dielectric mirror, 10Q20BB.3 was used to direct the light beam from the horizontal to the vertical direction, to illuminate the bottom-facing photoelectrodes. For nonaqueous experiments in CH_3CN, the photoelectrochemical behavior was determined in 1.0 M $LiClO_4$ with 50 mM $CoCp_2$ /10 mM $CoCp_2^+$, 25 mM $Me_{10}Cp_2Fc$/5 mM $Me_{10}Cp_2Fc^+$ and 90 mM Fc^0/0.5 mM Fc^+ redox systems, respectively, in an Ar-filled glovebox.

Electrochemical impedance spectroscopic data were obtained using a Biologic SP-200 potentiostat (Bio-Logic Science Instruments). Cyclic voltammetry, quantum yield, and stability data were obtained using a Biologic MPG-2-44 potentiostat (Bio-Logic Science Instruments). Cyclic voltammetric data were recorded at a 50 mV s^{-1} scan rate. External quantum yields were collected by connecting the potentiostat to a lock-in amplifier, with the light chopped at 20 Hz.

Electrochemical Impedance Spectroscopy and Mott-Schottky Analysis

Electrochemical impedance spectroscopy was conducted in the dark using n-Si/$SiO_{x,RCA}$/CoO_x samples in contact with a solution of 50 mM $K_3Fe(CN)_6$, 350 mM $K_4Fe(CN)_6$ and 1.0 M KCl(aq) ($E(Fe(CN)_6^{3-/4-}$ = 0.065 vs SCE). The data were fit to the model shown in Figure S0.

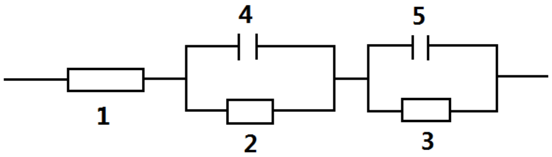

Figure S0 Equivalent circuit model used for fitting impedance data. 1, electrolyte resistance; 2, CoO_x resistance; 3, n-Si resistance; 4, CoO_x capacitance; 5, n-Si capacitance at the depletion layer.

The reverse-bias dependence of the area-normalized differential capacitance of the depletion-region of the semiconductor is given by the Mott-Schottky relationship:

$$\frac{1}{C^2} = \frac{2}{A^2 \varepsilon_0 \varepsilon_r q N_d}\left(V_{app} - V_{fb} - \frac{k_B T}{q}\right)$$

where V_{app} is the difference between the applied potential and the Nernstian potential of the solution, V_{fb} is the flat-band potential, k_B is Boltzmann's constant, *T* is the temperature in K, *A* is the device area, ε_0 is the vacuum permittivity, ε_r is the relative permittivity, *q* is the unsigned charge on an electron, and N_{d} is the donor impurity concentration in the semiconductor. The Mott-Schottky data were well fit by a linear relationship with $R^2 > 0.99$.

Measurements of Faradaic efficiency for the production of O_2:

The volume of the generated O_2(g) was measured using an eudiometer. The mass of the generated O_2(g) was calculated according to the immediate pressure and temperature of O_2(g) in the eudiometer. The reference electrode was a Hg/HgO/1.0 M KOH electrode and the counter electrode was a carbon rod, which was placed in a fritted compartment. The geometric area of the working electrode was ~0.75 cm^2, and the current was maintained at 5 mA. The light intensity at the position of working electrode was not calibrated to 1 Sun condition, due to the difficulty to measure the light intensity inside a eudiometer using a photodiode. Besides, the working electrode was placed far from the counter electrode, in order to be illuminated, so solution resistivity loss was high. As a result, the current density was low even if the electrode was biased at around 1.6 V versus RHE. The amount of oxygen generated versus time assuming 100% Faradaic efficiency was calculated by converting the charge passed into coulombs, then converting the value to the mass of O_2.

Transmission-electron microscopy (TEM)

Cross-sectional samples were mounted on Mo slot grids (SPI Supplies) with an M-Bond 610 adhesive. The samples were manually polished with diamond lapping film discs (Allied High Tech Products, Inc.), followed by further polishing with a dimpling machine (E.A. Fischione Instruments, Inc.), and finally thinned by Ar ion milling. TEM imaging was performed with an FEI Tecnai F30ST microscope with an accelerating voltage of 300 kV.

Atomic-force microscopy:

Atomic-force microscopy (AFM) was performed using a Bruker Dimension Icon operating in ScanAsyst mode to characterize the morphology of electrode surfaces. The ScanAsyst mode is based on the Peak-Force Tapping mechanism, performing a fast force curve capture at every pixel in the image, with the peak force of each curve used as the imaging feedback signal. Bruker ScanAsyst-Air probes (silicon tip, silicon nitride cantilever, spring constant: 0.4 N/m, frequency: 50-90 kHz) were used for n-Si/$SiO_{x,RCA}$/CoO_x electrodes. The scan size was 500 × 500 nm for the ScanAsyst mode. The images were analyzed using NanoScope Analyst software (version 1.40).

Calculations

Calculation of solar-to O_2(g) ideal regenerative-cell conversion efficiency (η_{IRC}):

Given the *J-E* data for a photoanode (potential vs RHE), the potential axis was converted to the potential relative to $E^{0\prime}(O_2/H_2O)$ by subtracting the value of *E* versus RHE from 1.23 V. The resulting potential was then multiplied by the corresponding current density at each point, and the maximum value of the product for the data was found and divided by the illumination intensity (in mW cm^{-2}) to yield the solar-to-O_2(g) ideal regenerative-cell conversion efficiency. Hence, the maximum value of (*E* vs $E^{0\prime}(O_2/H_2O)$) × *J*(at *E* vs $E^{0\prime}(O_2/H_2O)$) divided by illumination intensity (in mW cm^{-2}) yielded the solar-to O_2(g) ideal regenerative-cell conversion efficiency.

Definition of the terms "equivalent open-circuit voltage (V_{oc})" and "photovoltage"

The equivalent open-circuit voltage (V_{oc}) is the voltage that would need to be produced by a photodiode connected in series with a dark electrolysis cell to yield *J-E* behavior equivalent to that observed for the photoelectrode. In this work, photovoltage has the same meaning as equivalent open-circuit voltage.

Photocurrent density from integration against the AM 1.5G spectrum:

The integrated photocurrent density according to the measured external quantum yield under the spectral distribution of the standard AM 1.5G spectrum was calculated using the following equation:

$$J = \int_{\lambda=350}^{\lambda} {}^{q}/_{hc}\, \Phi_{\mathrm{ext}}(\lambda) \cdot E(\lambda) \cdot \lambda \cdot d\lambda \approx \int_{\lambda=350}^{\lambda} {}^{\Phi_{\mathrm{ext}}(\lambda) \cdot \lambda}/_{1240} \cdot E(\lambda) \cdot d\lambda \tag{S2}$$

where J is the integrated photocurrent density in A m^{-2}, q is the unsigned charge on an electron, E is the irradiance in W m^{-2} nm^{-1}, h is Planck's constant (6.63×10^{-34} J s), c is the speed of light (2.998×10^{8} m s^{-1}), Φ_{ext} is the measured external quantum yield, λ is the light wavelength in nm, 1240 is in W nm A^{-1}, and $\Phi_{\mathrm{ext}} \cdot \lambda/1240$ is the responsivity in A W^{-1}.

Supplementary discussions:

Discussions about the optimization of the CoO_x thickness for n-Si/$SiO_{x,RCA}$/CoO_x photoanodes:

Figure S7 shows that the n-Si/$SiO_{x,RCA}$/60C-CoO_x (~2 nm thick CoO_x) photoelectrodes exhibited photocurrent-onset potentials of -1 mV, -244 mV and -510 mV relative to the redox couple solution potentials, in contact with $Co(Cp)_2^{+/0}$ – 1.0 M CH_3CN, $Me_{10}Cp_2Fe^{+/0}$ – 1.0 M CH_3CN and $Fe(Cp)_2^{+/0}$ – 1.0 M CH_3CN, respectively. The photocurrent-onset potentials varied significantly (> 500 mV) as the solution potential changed, indicating that some regions of the Si surface were exposed to the solution during the non-aqueous electrochemical experiments. The n-Si/$SiO_{x,RCA}$/60C-CoO_x junction consisted of both low and high barrier-height regions, which reduced the overall open-circuit voltage of the n-Si/$SiO_{x,RCA}$/60C-CoO_x photoanode. Therefore, a thick (> 2 nm) CoO_x film would provide a higher photovoltage n-Si/$SiO_{x,RCA}$/CoO_x junction than a thin CoO_x film.

As the thickness of the CoO_x layer was increased up to > 600 ALD cycles, relatively little variation, within experimental error, was observed for the photocurrent-onset potentials for n-

Si/SiO$_{x,RCA}$/CoO$_x$ photoanodes, (Figure S1B). However, when the CoO$_x$ film was very thick (> 1000 ALD cycles or > 50 nm), the resistance of the film was large (Figure S1A).

Extended Stability of n-Si/SiO$_{x,RCA}$/CoO$_x$ photoanodes:

The 100-day stability under continuous operation is encouraging, but it is not practical to perform stability tests lasting a year on every interface of interest. Accelerated testing protocols are needed to address this issue including variations in temperature, changes that might occur due to diurnal cycles, and environmental effects that will determine the rest potential of the electrode in the dark as well as during periods of low illumination.

Supplementary Figures:

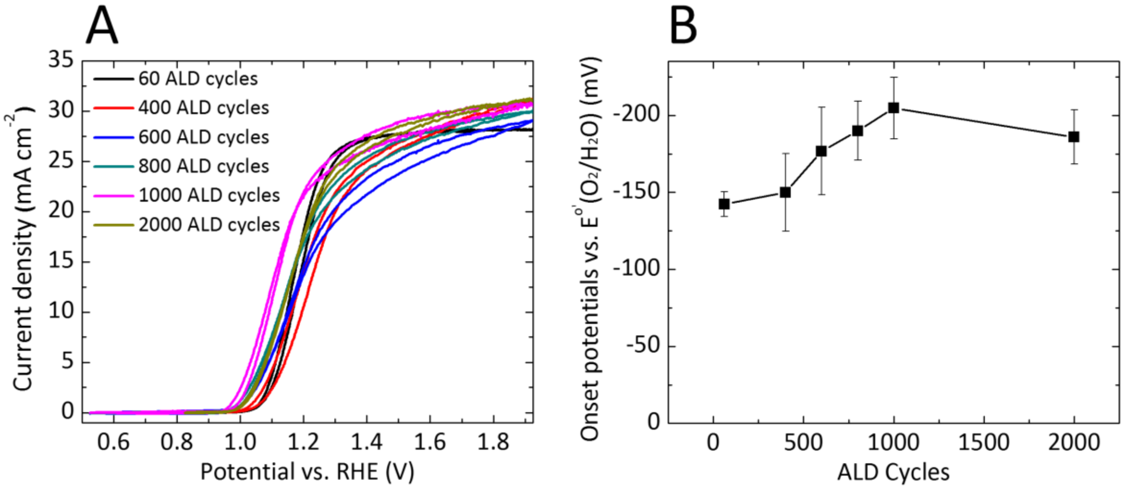

Figure S1 (A) Representative *J-E* behavior of n-Si/SiO$_{x,RCA}$/CoO$_x$ photoanodes with different CoO$_x$ thickness in 1.0 M KOH under 110 mW cm^{-2} of simulated solar illumination. (B) Dependence of photocurrent-onset potentials relative to the formal potential for the oxygenevolution reaction (OER) on the thickness of the CoO_x layer for n-Si/$SiO_{x,RCA}$/CoO_x photoanodes, as indicated by the number of ALD cycles used to deposit the coating.

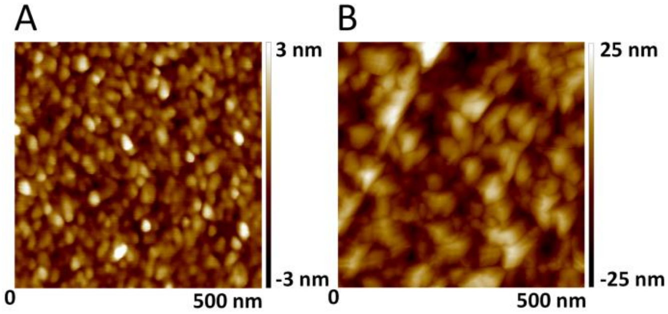

Figure S2 AFM image showing the surface morphology of an n-Si/$SiO_{x,RCA}$/CoO_x device (A) before and (B) after the PEC stability test biased at 1.63 V vs RHE under 1.1 Sun of simulated solar illumination in contact with 1.0 M KOH(aq). The root-mean-square surface roughnesses were (A) 0.74 nm and (B) 7.2 nm. The increased surface roughness indicated the dissolution of the CoO_x layer in 1.0 M KOH(aq) solution under bias and the possibility of pinholes formation. As results, the interface between CoO_x/Si would influence after long term stability test. The reasons of the performance decay would come from both catalyst degradation and interface changes.

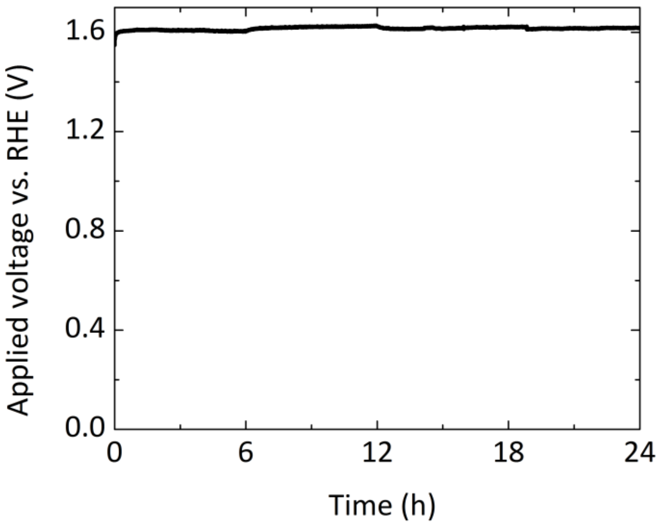

Figure S3 The voltage required to maintain 6.7 mA cm^{-2} of current density as a function of time for an n-Si/$SiO_{x,RCA}$/CoO_x photoanode in contact with 1.0 M KOH(aq) and under 1 Sun of simulated 1.5 G solar illumination.

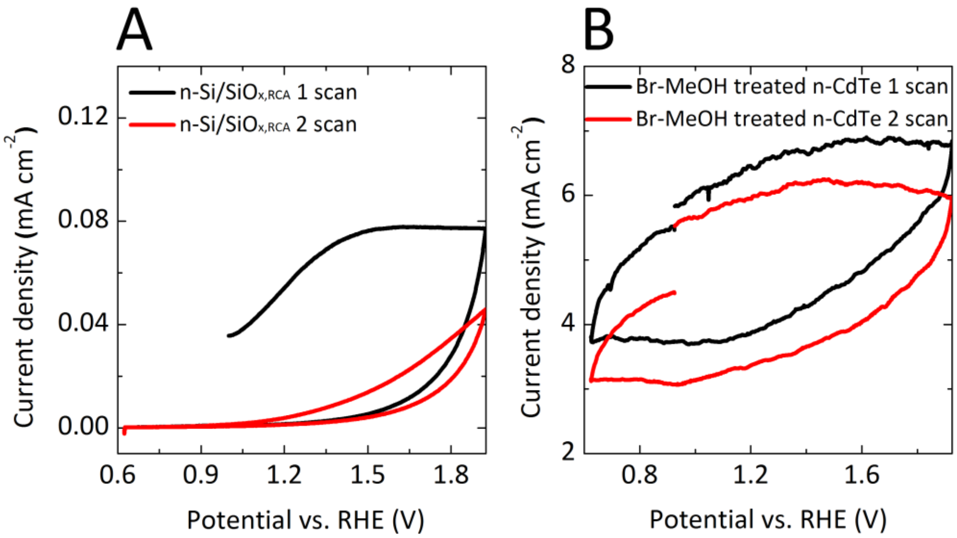

Figure S4 *J-E* data for etched n-Si/$SiO_{x,RCA}$ (A) and n-CdTe (B) photoelectrodes, without a CoO_x coating. Measurements were performed in 1.0 M KOH(aq) under 1 Sun of simulated illumination.

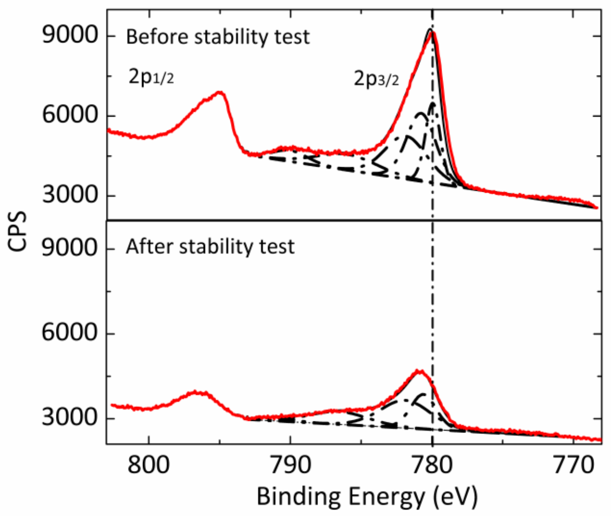

Figure S5 X-ray photoelectron spectroscopic (XPS) data for the n-Si/$SiO_{x,RCA}$/CoO_x photoanode before and after the PEC stability test biased at 1.63 V vs RHE under 1.1 Sun of simulated solar illumination in contact with 1.0 M KOH(aq). The binding energies used for fitting of the Co $2p_{3/2}$ peaks were 779.9 eV, 780.7 eV, 781.8 eV, 786.0 eV, 790.0 eV (before stability test), and 780.6 eV, 781.9 eV,786.6 eV, 790.8 eV (after stability test). Peak fitting of the XPS spectra before the stability test in the Co $2p_{3/2}$ region and grazing incidence X-ray diffractometry (GIXRD) in previous work showed the existence of Co_3O_4.[2-4] The shift of the Co 2p core level emission to higher binding energy indicated the transformation from Co_3O_4 to CoOOH.[5]

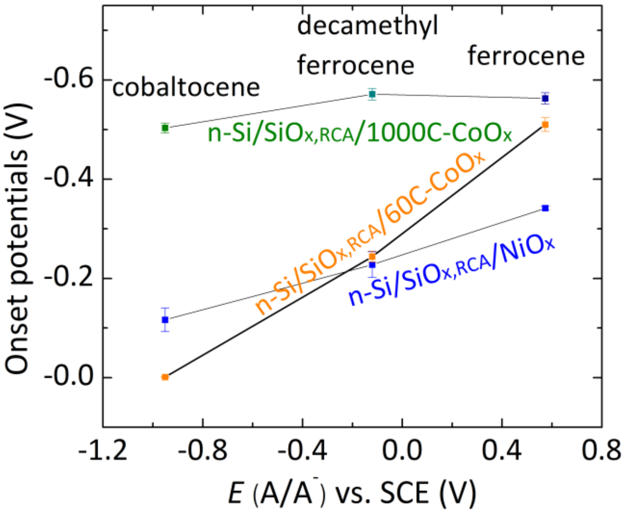

Figure S6 Photocurrent-onset potentials versus the Nernstian potential of the solution for n-Si/$SiO_{x,RCA}$/60C-CoO_x (60 ALD cycles, 2 ~ 3 nm thick CoO_x) (orange), n-Si/$SiO_{x,RCA}$/1000C-CoO_x (1000 ALD cycles, ~50 nm thick CoO_x) (green) and n-Si/$SiO_{x,RCA}$/NiO_x (~100 nm thick sputtered NiO_x) (blue) photoelectrodes under 100W cm^{-2} illumination in cobaltocene, decamethyl ferrocene, and ferrocene redox systems, respectively. The data indicate the change in the observed photovoltage as the redox potential of the solution was varied. Lines only connect the experimentally observed values; no functional form is assumed.

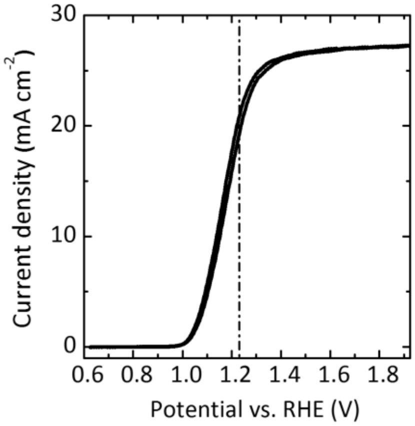

Figure S7 Representative *J-E* behavior of planar n-Si/$SiO_{x,RCA}$/100C-CoO_x photoanodes with 100 ALD cycles of CoO_x in 1.0 M KOH(aq) under 1 Sun simulated illumination.

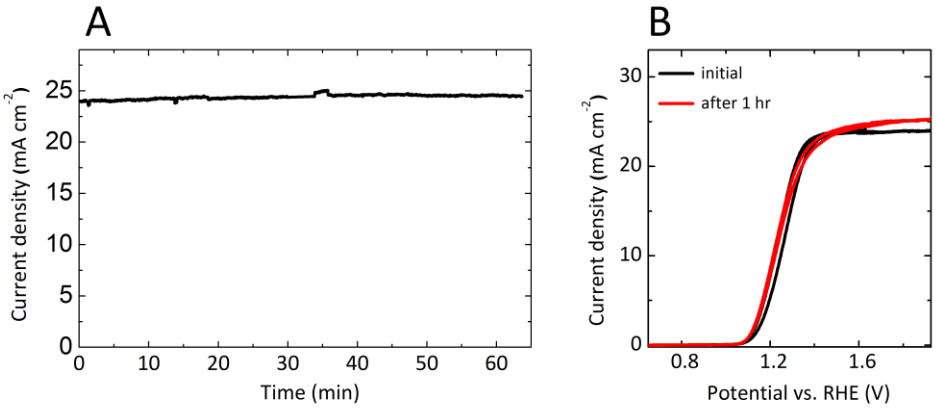

Figure S8 (A) Chronoamperometry curve of n-Si/$SiO_{x,RCA}$/CoO_x (60 ALD cycles for CoO_x) photoanode biased at 1.63 V vs RHE under 1 Sun of simulated 1.5G solar illumination from an ENH-type tungsten-halogen lamp. (B) *J-E* data for planar n-Si/$SiO_{x,RCA}$/CoO_x (60 ALD cycles for

CoO_x) in contact with 1.0 M KOH(aq) under 100 mW cm^{-2} of simulated 1.5 G solar illumination collected before and after the stability test shown in Figure S3B.

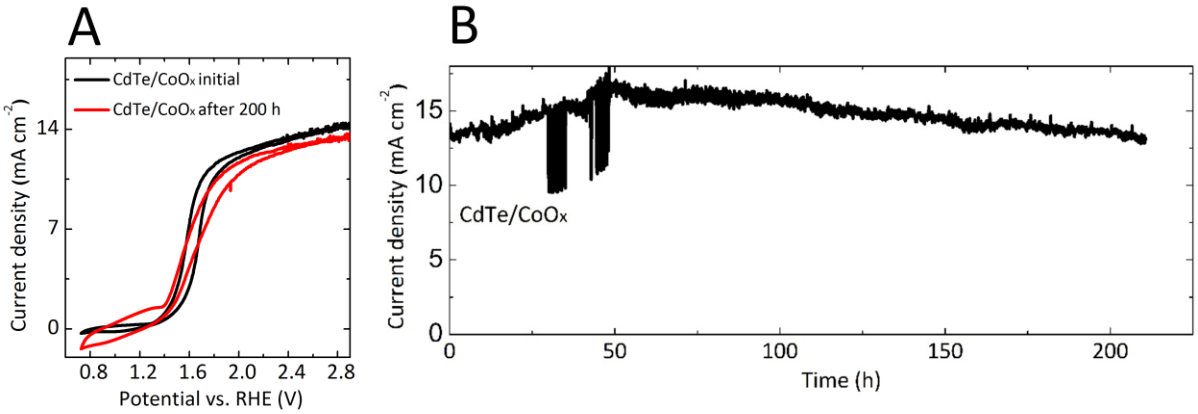

Figure S9 (A) *J-E* data for an n-CdTe/1000C-CoO_x (1000 ALD cycles) photoanode in 1.0 M KOH(aq) under 1 Sun of simulated 1.5G solar illumination before and after 200 h of continuous operation at 2.8 V vs. RHE. (B) Chronoamperometry of n-CdTe/1000C-CoO_x photoanode biased at 2.8 V vs. RHE under 1 Sun of simulated 1.5G solar illumination in contact with 1.0 M KOH(aq).

References

1. H. B. Gray, D. N. Hendrickson and Y. S. Sohn, *Inorg. Chem*, 1971, **10**, 1559-1563.
2. J. Yang, H. Liu, W. N. Martens and R. L. Frost, *J. Phys. Chem. C*, 2010, **114**, 111-119.
3. M. C. Biesinger, B. P. Payne, A. P. Grosvenor, L. W. M. Lau, A. R. Gerson and R. S. C. Smart, *Appl. Surf. Sci.*, 2011, **257**, 2717-2730.
4. X. Zhou, R. Liu, K. Sun, D. Friedrich, M. T. McDowell, F. Yang, S. T. Omelchenko, F. H. Saadi, A. C. Nielander, S. Yalamanchili, K. M. Papadantonakis, B. S. Brunschwig and N. S. Lewis, *Energy Environ. Sci.*, 2015, **8**, 2644-2649.

5. J. Yang, K. Walczak, E. Anzenberg, F. M. Toma, G. Yuan, J. Beeman, A. Schwartzberg, Y. Lin, M. Hettick, A. Javey, J. W. Ager, J. Yano, H. Frei and I. D. Sharp, *J. Am. Chem. Soc.*, 2014, **136**, 6191-6194.